Chem. Phys. Reports, 1996, Vol. 15(2), p. 301-309
Reprints available directly from the publisher
Photocopying permitted by license only

THE SHAPE OF ESR LINES, KINETIC PARAMETERS OF CONDUCTION ELECTRONS, AND THEIR CHANGES IN TWO-DIMENSIONAL CRYSTALLIZATION OF MOLECULES INCORPORATED IN INTERCALATION GRAPHITE COMPOUNDS

A.M. ZIATDINOV and N.M. MISHCHENKO
Institute of Chemistry, Far East Division of Russian Academy of Sciences, Vladivostok, Russia

(Received February 10, 1994)

Applicability of the one-dimensional Dyson equations for the ESR line of conduction electrons (CE) in isotropic metals to analyzing the ESR spectrum of CE in plates of a quasi-two-dimensional highly anisotropic conductor — intercalated graphite compound (IGC), $C_{20}HNO_3$, is proved experimentally. ESR data are used to estimate some kinetic parameters of spin carriers and conductivity along the c axis before and after crystallization of the "guest" molecules. Crystallization of two-dimensional layers is shown to occur in two stages and is attended by reduction of the spin-carrier mobility, enhancement of electric conductivity, and some redistribution of the electron density between the carbon and intercalated-material subsystems.

INTRODUCTION

In recent years the CE ESR method has been often employed to study intercalated graphite compounds (IGC), which are an alternating sequence of n-hexagonal graphite layers (n is the so-called intercalation stage index) and layers of "guest" (intercalated) molecules [1—10]. However IGC are anisotropic conductors: in acceptor and donor IGC, the ratios between conductivities along and perpendicular to the carbon layers, σ_a/σ_c, are $\sim 10^5$ and ~ 10, respectively [11]. Therefore the question concerning validity of the well-known theory developed by Dyson [12] and Kaplan [13] for infinite isotropic metal plates of an arbitrary thickness with a single-type current carrier and modified in [14, 15, 16] to treat conductivity in isotropic metals of finite size still remains open. The lack of an experimentally substantiated method for analyzing the shapes of CE ESR lines of highly anisotropic conductors prevents extensive use of the above approaches in investigations of physicochemical processes taking place in IGC.

In this work we present experimental results of investigations into correlation between the shape of CE ESR lines recorded in plates of IGC α-modification with nitric acid of the fourth stage, $C_{5n}HNO_3$ ($n = 4$), and (1) sample size, (2) orientation of the constant magnetic field H_0 with respect to the c axis of the graphite matrix, (3) mode of the microwave field, and (4) phase state of the intercalated compound (in $C_{5n}HNO_3$ two-dimensional liquid-like HNO_3 layers are crystallized at $T_c = 250$ K [11, 17]). The experimental data proved applicability of the one-dimensional Dyson equations [12] to analyzing ESR CE spectral lines of a highly anisotropic $C_{20}HNO_3$ conductor. The CE ESR data were

used to evaluate some kinetic parameters of the spin carriers and σ_c. They have revealed that upon intercalated-compound crystallization the mobility of spin carriers along the basic plane reduces, while their concentration increases. This is indication of some redistribution of the electron density among the graphite and intercalated-material subsystems. Crystallization of the lattice liquid in IGC studied was shown to proceed in two stages (via an intermediate state).

EXPERIMENTAL

CE ESR spectra of $C_{20}HNO_3$ IGC plates were recorded on an ESR-231 radio-spectrometer (Academy of Sciences of former DDR) in the X range (ν = 9.52 GHz) in a rectangular cavity with the TE_{102} mode at a frequency of the H_0 field ν_m = 2.5 kHz. With a conventionally mounted cavity, the vector of the electrical component of the microwave field $\vec{E}_\eta$ is parallel to H_0; in the geometric center of the cavity the magnetic-component vector $\vec{H}_\eta$ of the microwave field is parallel to the vertical cavity axis, and the Pointing vector $\vec{P}$ lies in a horizontal plane and is perpendicular to H_0. To elucidate the effect of the geometry of microwave-field lines of force on the line shape, CE ESR spectra in the X-range at 300 K were recorded also in a cylindrical cavity (the H_{011} mode).

All the plates of highly oriented pyrolytic graphite (HOPG) used in synthesis of IGC were cut from one rod, whose conductivity along the basic plane was $(1.2 \pm 0.2) \cdot 10^4$ $Ohm^{-1} \cdot cm^{-1}$, they had a shape of parallelepipeds of a size l(width) × h(height) × d(thickness); $l \times h$ is the area of the base face. The plate sizes were measured with an accuracy of $5 \cdot 10^{-4}$ cm.

IGC with HNO_3 of the fourth intercalation phase were synthesized from two series of HOPG plates: (1) with l varying from 0.032 to 0.315 cm at constant h = 0.505 cm and d = 0.018 cm and (2) with d varying from 0.024 to 0.043 cm at constant h = 0.0505 and l =0.323 cm in nitric acid with a density ρ = 1.492 cm^{-3}. The IGC stage was controlled by the diffraction technique. According to measurements by this technique, the distance between the carbon layers adjacent to the intercalated material is (7.79 ± 0.0 1) Å. Measured differences of the plate weight prior to and after intercalation in them of nitric acid molecules indicate that the compound formula is $C_{20\pm1}HNO_3$. Based on these characteristics, the synthesized compounds were referred to the fourth stage of IGC α-modification with HNO_3, representatives of which are described by a general formula $C_{5n}HNO_3$ (n = 1, 2, 3, ...) [11, 17]. The planes of HNO_3 molecules were oriented in this modification nearly perpendicular to carbon layers [11].

IGC plates were placed in sealed quartz ampoules and oriented in such a way that their c axis was perpendicular and the vertical faces parallel to $\vec{H}_\eta$. Samples were placed at nodes of $\vec{H}_\eta$ (in the geometric center of the cavity).

CE ESR spectra of IGC plates were taken in a temperature range 200—300 K. The temperature was varied by gaseous nitrogen flowing at controlled rates and temperatures through a quartz Dewar vessel containing a sample. In the vicinity of T_c the temperature was varied step-wise at steps ΔT = 0.2° and was maintained to within 0.1 degree/h. The dependence of the shape of CE lines in ESR spectra of IGC plates on their size was studied at 300 and 220 K.

The values of σ_a of synthesized IGCs were determined by a nonitrusive induction technique on a set-up schematically depicted in [18].

EXPERIMENTAL RESULTS

CE ESR spectrum of IGC $C_{20}HNO_3$ exhibits a single signal throughout the temperature range studied, the phase of the line shape is "normal" in the sense that the more intense wing of the signal with a peak intensity A is positioned in lower magnetic fields than the less intense wing of a peak intensity B. At a given temperature and l, the values of A/B and CE ESR line shape ΔH, as measured at the half-width of the peak A, is independent of h, d, the mode of microwave field, and plate orientation with respect to $\mathbf{H}_0$. The spectrum is axially symmetric relative to c, the principal values of its g-tensor as determined by the procedure suggested in [14] or [15] are temperature independent: $g_\parallel = 2.0023 \pm 0.0001$ and $g_\perp = 2.0028 \pm 0.0001$. At $\mathbf{H}_0 \perp (\parallel)$ c, the ratio of the integral signal intensities calculated by formula $I = (A + B)\Delta H^2$ for both cavities is 11: 10. The weak angular dependence of I on orientation of the IGC plates with respect to $\mathbf{H}_0$ observed in both rectangular and cylindrical cavities is attributable to interaction of the electron IGC subsystem with $\mathbf{H}_0$ rather than with the microwave field.

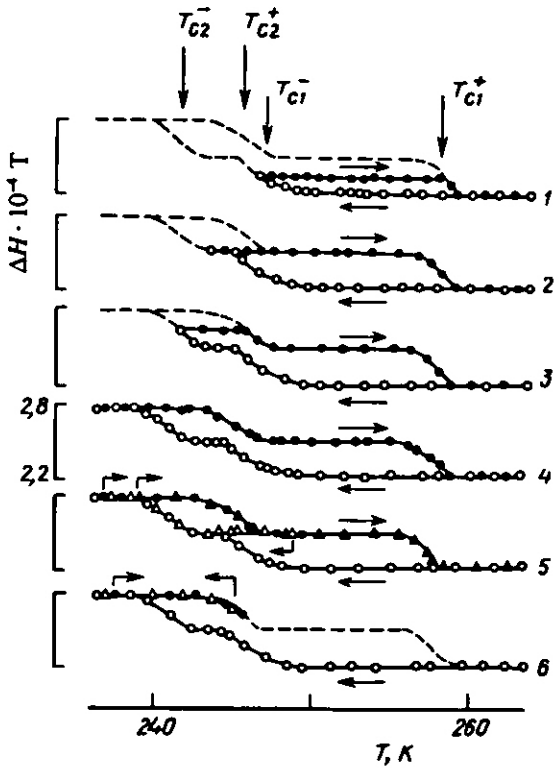

FIGURE 1. Temperature dependence of the CE ESR line ΔH recorded in $C_{20}HNO_3$ samples with a crystallizing (melting) intercalated compound. Open symbols signify parameters measured in cooled (heated) IGC samples. Curves *1*—*6* pertain to different limiting temperatures of intercalated-material transition from liquid phase to the solid state; T_{c1}-(T_{c1}^+) and T_{c2}-(T_{c2}^+) are the temperature of the first and second step-wise changes ΔH upon cooling (heating) of the sample, respectively. The arrows indicate temperature changes along the respective curves; $\mathbf{H}_0 \perp$ c, $\nu = 9.52$ GHz.

The A/B and ΔH values are temperature-independent up to 250 K and are equal to 3.2

± 0.2 G and 2.2 G, respectively. As the temperature is lowered further, the ΔH value rises in two steps (Fig. 1). In the range where ΔH changes step-wise the $d(\Delta H)/dT$ derivative peaks at T_{c1-} = (247 ± 0.3) K and T_{c2-} = (242 ± 0.3) K. As the temperature rises, ΔH and A/B change in the reverse order, however with an "overall" temperature hysteresis. In particular, ΔH reduces most rapidly at T_{c2}^{+} = (245 ± 0.3) K and T_{c1}^{+} = (258 ± 0.3) K (Fig. 1). Irrespective of the direction of temperature variations, transitions between various sections of the $\Delta H(T)$ curve (its kinks) are observed at approximately one and the same temperature (Fig. 1). The temperature hysteresis of the regions of step-wise changes in $\Delta H(T)$ suggests that these variations can be considered as first-order phase transitions. The value of I increases ~1.4-fold as the temperature decreases from 300 to 220 K. According to the literature data [11, 17], in $C_{3n}HNO_3$, the temperature of crystallization (melting) of two-dimensional intercalated-material layers T_c = 250 K, therefore alterations of the CE ESR lines recorded in $C_{20}HNO_3$ at temperatures close to the above-indicated value are assumed below to be caused by changes of the phase state of the "guest" molecular subsystem. At powers far below the saturating power and at identical temperatures the ΔH value in the Q-range is 7% higher than that in the X-range.

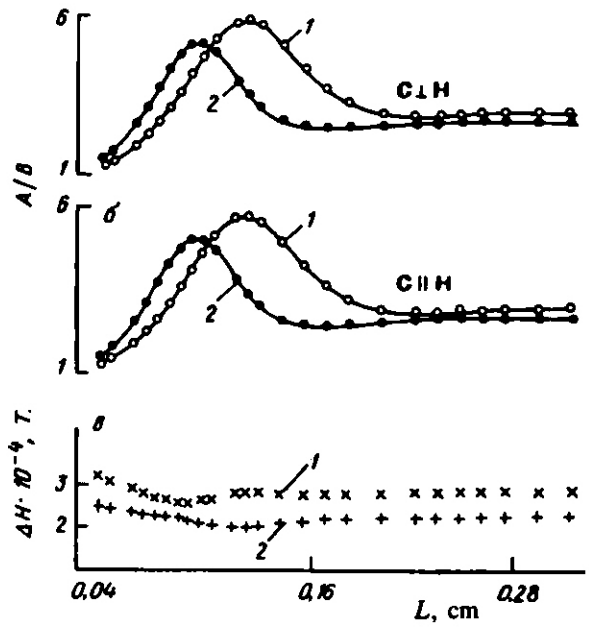

FIGURE 2. Asymmetry parameter A/B (*a*, *b*) and width ΔH (*c*) of CE ESR lines for $C_{20}HNO_3$ plates of size $l \times 0.505 \times 0.018$ cm^3 versus l at 300 K (*1*) and 220 K (*2*) and at ν = 9.52 GHz. The theoretical curves at 300 (200) K were calculated by Dyson's equation for the line shape with σ_c = 1.6(2.7) Ohm$^{-1}\cdot$cm^{-1}, R_a = 1.2(1.8), and $T_2 = 2.84(2.13)\cdot 10^{-8}$ s.

The dependences of A/B on l are similar at 300 and 220 K; as $l \to 0$, it passes through a minimum that precedes the maximum, and at large l values it levels off (Fig. 2, *a*, *b*). At $T >$ (<) T_c the A/B values at the maximum corresponding to l_{max} = 0.12(0.085) cm, at the minimum corresponding to l_{min} = 0.22(0.16) cm, and on the plateau attained at l > 0.36(0.28) cm are equal to: 5.8 ± 0.2 (5.1 ± 0.2), 2.9 ± 0.2 (2.5 ± 0.2), and 3.2 ± 0.2 (2.8 ± 0.2), respectively. The $\Delta H(l)$ dependence resembles in general features the A/B versus l dependence, however, as $l \to 0$, starting with $l > l_{max}$, ΔH slightly rises (Fig. 2, *c*) which is attributed to transformation of the Dyson line shape to the Loretzian one.

The σ_c value for C_2HNO_3 plates at lower temperatures increases from $\sim 3.2 \cdot 10^5$ Ohm^{-1} at 300 K to $\sim 4.1 \cdot 10^5$ $Ohm^{-1} \cdot cm^{-1}$ at 200 K.

DISCUSSION

The Fermi level in IGC at $n > 1$ crosses several bands [11, 19, 20]. However, because of averaging over the Fermi surface on the scale of ESR times, various states of the current carriers in IGC are indiscernible [1—11, 20]. This allows $C_{20}HNO_3$ IGC to be considered in ESR experiments as a conductor with a single type current carrier.

In isotropic metals with a single type current carrier, if the average free path length of electrons is much shorter than the skin-layer thickness δ (the so-called "normal" skin-effect), the skin-layer thickness is related to the frequency by the well-known equation $\delta = c/(2\pi\sigma\nu)^{1/2}$, where c is the velocity of light. The family of curves depicting the asymmetry parameter A/B of the CE ESR line versus the thickness L of the metal plate reduced by δ at different values of the ratio $R = (T_D/T_2)^{1/2}$ (T_D is the time of spin-carrier diffusion through the skin-layer δ and T_2 is the time of spin-lattice relaxation) calculated by the authors for this case using one-dimensional Dyson's equation for the line shape in isotropic metals $F(\sigma, T_2, R, L)$ [12] is displayed in Fig. 3. In further interpretation of the experimental data of interest are only curves with $R > 0.55$. These curves show similar A/B versus L/δ dependences with a single peak and at great L/δ values level off at $2.55 \leq A/B < 5$. As $L\delta \to 0$, they pass through a minimum which precedes the maximum. Nomograms calculated by the Dyson equation for the line shape [12] and intended for determining, at $R > 0.55$, the L/δ value corresponding to the appropriate extremum from the $A/B(L)$ values at the minimum and maximum, the R values at the extremum points from the L/δ magnitudes and the R value from the $A/B(L)$ magnitude on the plateau are presented in Fig. 4.

In the rectangular cavity with the TE_{102} mode at $\mathbf{H}_0 \parallel (\perp)$ c, provided that the configuration and density of lines of forces in th cavity are only sligntly perturbed by loading it with a sample, " is perpendicular to the vertical faces $h \times d(h \times l)$ and the microwave field must be absorbed only through these faces. Obviously, if the above assumption is valid, the l and A/B values for a resonance signal must be heavily dependent on the plate orientation with respect to the lines of forces of the microwave field, because of the large anisotropy of the acceptor-IGC conductivity ($\sim 10^5$ [11]). As mentioned above, no such dependences were observed in experiments with $C_{20}HNO_3$ plates. This fact, as well as the identity of shapes of the CE ESR lines in rectangular and cylindrical cavities indicate that the dominating contribution to formation of the microwave field in neighborhood of the IGC plate surfaces is made by the plates themselves. In other words, *a priori* there is no grounds to believe that $\tilde{\mathbf{H}}_{\eta}$ near the vertical faces of IGC plates is homogeneous. However, this does not necessarily mean that the lack of data on the $\tilde{\mathbf{H}}_{\eta}$ distribution near the IGC-plate surface in the case considered impedes analyzing the CE ESR line shape. Indeed, independence of the CE ESR line shape from d and h and similarity of the $A/B(l)$ and $\Delta H(l)$ curves at $\mathbf{H}_0 \parallel (\perp)$ c (Fig. 2) indicate that at all l values the microwave field is absorbed by the plates predominantly through their vertical faces parallel to c, whatever their orientation. In other words, in the series of IGC plates studied a type of $\mathbf{H}_{\eta}$ distribution near the vertical faces does not affect, within the experimental accuracy, the CE ESR line contour, because of the negligibly small contribution to the resonance of the zones adjacent to the base faces. Hence, the line shape can be described by the one-dimensional Dyson equation for the CE ESR line shape in isotropic metals: $F(\sigma_c, R_e, T_2, l)$ [12], where $R_e = (T_{De}/T_2)^{1/2}$ (T_{De} is the time of spin-

carrier diffusion along the base plane through the skin-layer δ depending on conductivity σ_c.

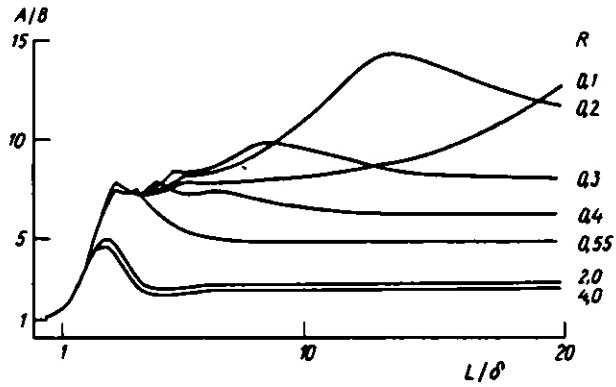

FIGURE 3. Theoretical dependences of the asymmetry parameter A/B of the ESR line of mobile spin carriers on the plate thickness reduced by the skin-layer thickness at various values of $R = (T_D T_2)^{1/2}$ calculated by the Dyson equation for the line shape [12].

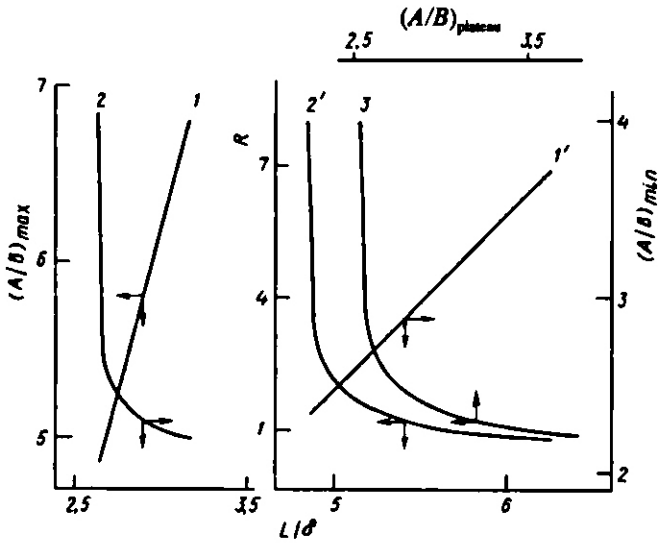

FIGURE 4. Theoretical curves for evaluating (*i*) L/δ at the extremum from the asymmetry parameter $A/B(L)$ at the maximum (minimum) and curve (*1* or *1'*), (*ii*) R from the L/δ value at the maximum (minimum) and curve (*2* or *2'*), (*iii*) R from the $A/B(L)$ value and curve *3*.

The single-peak dependence of A/B on l levelling off at large l with $A/B < 5$ and passing through a minimum preceding the maximum as $l \to 0$ (Fig. 2, *a*) suggests that in $C_{20}HNO_3$ $R_a > 0.55$ both prior to and after crystallization in it of the intercalated material. Therefore, σ_c and R_a values were estimated from the nomograms shown in Fig. 4 and determined from the experimental values of A/B at the maximum or minimum of the A/B versus l dependences. R_a can also be evaluated from the A/B values on the plateau of the same curve. All the above versions of estimation of the desired parameters at 300 (220) K yield the same values of $\delta_c = 0.041$ (0.031) cm, $\sigma_c = 1.6$ (2.7) $Ohm^{-1} \cdot cm^{-1}$, and

R_a = 1.2 (1.8). The value of T_2 at 300 (220) K calculated from the relation $T_2 = (g_\perp\beta/\hbar)\Delta H$ (where β is the Bohr magneton, ΔH is the CE ESR line width measured in IGC plates with l corresponding to the plateau portion of the A/B dependence on l) equals 2.84(2.10) · 10^{-8} s. Note that at 300 K the σ_c value for IGC studied is about 4.5 times as low as the value of the appropriate component of HOPG conductivity [21, 22] and nearly equal to the magnitude of σ_c reported in the literature for C_5HNO_3 plates at the same temperature (~ 1.8 $Ohm^{-1} \cdot cm^{-1}$ [23]). Numerical modeling of experimental A/B versus l dependences and CE ESR line contours for $C_{20}HNO_3$ IGC plates performed with the use of the one-dimensional Dyson equation for the line shape $F(\sigma_c, T_2, R_a, l)$ with substitution in it of the found σ_c, T_2, and R_a values shows a fairly good fit of calculations to the experimental curves (Figs. 2, *a*, *b* and 5). Known the R_a and T_2 values at 300 (200) K T_{Da} is easily estimated at 2.09(9.52) · 10^{-8} s by the nomograms calculated in [14]. According to Dyson [12], in the approximation of independent electrons the T_D value is related with the diffusion constant D of spin carriers by equation $D = \delta^2/2T_D$. In turn, mobility μ is related to D by the second Einstein equation derived for diffusion processes: $\mu = eD/kT$. By analogy, from these three equations one can calculate the diffusion constant D_a and mobility μ_a of spin carriers along the graphite layers in $C_{20}HNO_3$. These calculations yield at 300 (200) K the following values: D_a 2.06(7.1) · 104 $cm^2 \cdot s^{-1}$ and μ_a = 6.9(3.7) · 105 $cm^2/(V \cdot s)$. As is seen, crystallization of the intercalated material reduces μ_a and increases σ_a. This contradictory result is attributed to the temperature dependence of l. Indeed, at a preset geometry of a sample $I \propto N\delta_c$, where N is the concentration of current carriers. Therefore the increase in I attended by decrease of δ observed upon crystallization of the intercalated compound points unequivocally to the increase of N.

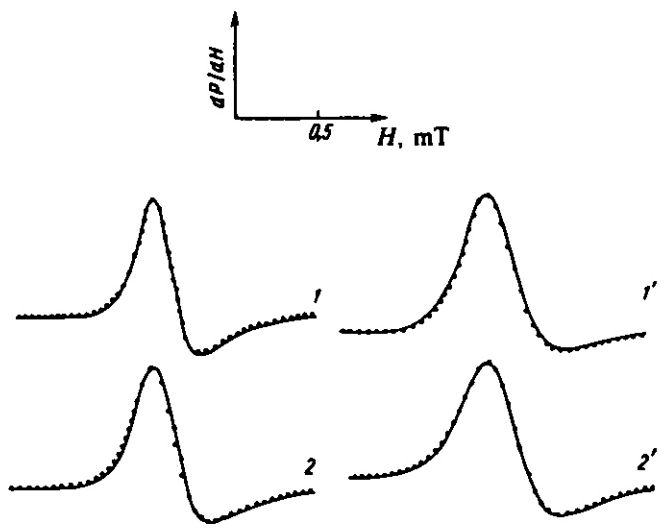

FIGURE 5. Comparison of experimental (solid line) and theoretical (dashed line) of the first derivative of an ESR absorption signal for $C_{20}HNO_3$ IGC plates of size $l \times 0.505 \times 0.043$ cm^3 at l = 0.073 (*1*, *1'*) and 0.294 cm (*2*, *2'*) and T = 300 (*1*, *2*) and 220 K (*1'*, *2'*); $H_0 \perp c$; ν = 9.52 GHz. The theoretical curves at 300 (220) K are calculated by the Dyson equation for the line shape [12] with σ_c = 1.6 (2.7) $Ohm^{-1} \cdot cm^{-1}$, R_a = 1.2 (1.8) and T_2 = 2.84 (2.10) · 10^{-8} s.

The frequency independence of ΔH both in quasi-liquid and solid phases of the intercalated material in $C_{20}HNO_3$ indicates that the CE ESR lines of this compound are broadened homogeneously. The principal values of the g-tensor of spin carriers in the IGC

studied which are close to the g-factor of a free electron and their independence from the phase state of the intercalated material suggest that the probability density of spin carriers on intercalated molecules is low and does not change upon phase transition. This supports applicability of the model of hard IGC bands [11, 19] to analyzing changes in the electronic properties of $C_{20}HNO_3$. Within the framework of this model, the N value may increase with lowering the temperature in acceptor IGC, referred to as conductors with a hole Fermi surface [11], solely when the Fermi level lowers due to "removal" of the additional electron density from the graphite layers [11, 24]. In other words, crystallization (melting) of the lattice liquid in $C_{20}HNO_3$ induces in it an oxidation (reduction) reaction. In $C_{5n}HNO_3$ IGC, the negative charge in the layer of intercalated material is carried by NO_3^- fragments surrounded by neutral HNO_3 molecules [11, 25]. Therefore an increase in the NO_3^- concentration may be one of the forms of charge localization during crystallization of the intercalated material. Since localized charges are scattering centers for conduction electrons, an increase in N must, obviously, be attended by a decrease in μ_e and an increase in ΔH. In other words, the model of hard bands in IGC predicts qualitatively correct changes in σ_e and ΔH upon crystallization of the subsystem of guest molecules, which is a solid argument in favor of its applicability to interpreting the experimental data.

It follows from the $\Delta H(T)$ dependence in the critical temperature region (Fig. 1) that two-dimensional melting of the intercalated materials proceeds via some intermediate state, i.e., is a two-stage process. Because the structural data in the range where the intermediate phase exists are lacking, identification of this phase is impeded. Nonetheless, we can make some guess concerning its nature. Indeed, the theory of two-dimensional melting [26] suggests that in ideal two-dimensional systems (with a zero potential of the support) transition from the solid phase to liquid proceeds through an intermediate "hexatic" phase. This phase is characterized by quasi-ideal orientational ordering and by the lack of positional ordering [26]. When the effect of support is neglected, transitions both from the solid phase to the "hexatic" phase and from the latter phase to liquid are continuous, whereas when interaction with the support is significant, these two transitions may occur jump-wise [26]. In $C_{5n}HNO_3$ in the quasi-liquid phase of intercalated HNO_3 molecules they rotate about the carbon—oxygen bond [25, 27] and execute translational hops between the positions preset by the periodical Coulomb potential generated by graphite layers adjacent to intercalated molecules [27]. In the solid phase of intercalated material the two above-indicated modes of HNO_3 molecular motions are frozen [27]. Based on these data, we may suppose that the intermediate phase revealed in $C_{20}HNO_3$ resembles the "hexatic" phase, that is, in this state the intercalated molecules presumably execute translational hops, but their rotations are still frozen.

Thus, the experimental substantiation of feasibility of application of the one-dimensional Dyson theory [12] to analyzing the CE ESR line shape in plates of quasi-two-dimensional highly-anisotropic synthetic $C_{20}HNO_3$ conductor made it possible to evaluate some kinetic parameters of spin carriers and σ_c in this compound. In turn, the analysis of the temperature dependence of these parameters has revealed previously unknown aspects of two-dimensional melting of intercalated material in the Coulomb potential generated by the adjacent carbon layers.

The authors are indebted to V.V. Sereda for modification of the set-up designed for measuring electric conductivity and to L.B. Nepomnyashchii (Research Institute for Graphite) for kindly supplied HOPG plates used to synthesize IGC. The experimental data were analyzed and interpreted by A.M. Ziatdinov.

REFERENCES

1. K.A. Müller and R. Kleiner, *Phys. Lett.* **1**, No. 1, 98 (1962).
2. S.K. Khanna, E.R. Falardeau, A.J. Heeger, and J.E. Fischer, *Sol. Stat. Commun.* **25**, No. 12, 1059 (1978).
3. P. Lauginie, H. Estrade, J. Conard, et al., *Physica* **99B**, No. 3, 514 (1980).
4. R. Davidov, O. Milo, I. Palchan, and H. Selig, *Synth. Met.* **8**, No. 1, 83 (1983).
5. I. Palchan, D. Davidov, V. Zevin, et al., *Synth. Met.* **12**, No. 5, 413 (1985).
6. R.M. Stein, L. Walmsley, and C. Rettori, *Phys. Rev. B* **32**, No. 6, 4134 (1985).
7. A.M. Ziatdinov, A.K. Tsvetnikov, N.M. Mishchenko, and V.Yu. Glushchenko, *Khim. Fiz.* **8**, No. 12, 1680 (1989).
8. M. Saint-Jean and E. McRae, *Phys. Rev. B* **43**, No. 5, 3969 (1991).
9. A.M. Ziatdinov, N.M. Mishchenko, and Yu.M. Nikolenko, *Synth. Met.* **59**, No. 2, 253 (1993).
10. A.M. Ziatdinov, *Ferroelectrics (USA)* **155**, No. 1—3, 383 (1994).
11. M.S. Dresselhaus and G. Dresselhaus, *Adv. Phys.* **30**, No. 2, 139 (1981).
12. F.J. Dyson, *Phys. Rev.* **98**, No. 2, 349 (1955).
13. J.I. Kaplan, *Phys. Rev.* **115**, No. 3, 575 (1959).
14. G. Feher and A.F. Kip, *Phys. Rev.* **98**, No. 2, 337 (1955).
15. H. Kodera, *J. Phys. Soc. Jpn.* **28**, No. 1, 89 (1970).
16. J.H. Pifer and R. Magno, *Phys. Rev.* **3**, No. 3, 663 (1971).
17. M.J. Bottomly, G.S. Parry, and A.R. Ubbelohde, *Proc. Roy. Soc. London* **A279**, No. 291, 291 (1964).
18. L.A. Pendrys, C. Zeller, and F.L. Vogel, *J. Mat. Sci.* **15**, No. 12, 2103 (1980).
19. S.Y. Leung and G. Dresselhaus, *Phys. Rev. B* **24**, No. 5, 3490 (1981).
20. K. Sugihara, K. Matsubara, and T. Tsuzuku, *J. Phys. Soc. Jpn.* **53**, No. 2, 795 (1984).
21. J,E, Fischer, C.D. Fuerst, and H.J. Kim, *J. Mat. Res. Soc. Symp. Proc.* **20**, 169 (1983).
22. A.M. Ziatdinov and N.M. Mishchenko, *Fiz. Tverd. Tela* **29**, No. 9, 2849 (1987).
23. A.R. Ubbelohde, *Proc. Roy. Soc. London A* **321**, No. 3, 445 (1972).
24. S. Loughin, R. Grayeski, and J.E. Fisher, *J. Chem. Phys.* **69**, No. 8, No. 8, 3740 (1978).
25. J. Conard, H. Fuzellier, and R. Vangelisti, *Synth. Met.* **23**, No. 2, 277 (1988).
26. K.J. Strandburg, *Rev. Modern Phys.* **60**, No. 1, 161 (1988).
27. F. Batallan, I. Rosenman, A. Magerl, and H. Fuzellier, *Phys. Rev. B* **32**, No. 7, 4810 (1985).